Available online at www.sciencedirect.com
ScienceDirect
International Journal of Heat and Mass Transfer 51 (2008) 2029–2040
International Journal of HEAT and MASS TRANSFER
www.elsevier.com/locate/ijhmt

Vascularization with trees matched canopy to canopy: Diagonal channels with multiple sizes

J. Lee [a], S. Kim [a], S. Lorente [b], A. Bejan [a,*]

[a] Department of Mechanical Engineering and Materials Science, Duke University, Durham, NC 27708-0300, USA
[b] Laboratory of Materials and Durability of Constructions, Department of Civil Engineering, National Institute of Applied Sciences, 135 Avenue de Rangueil, 31077 Toulouse, France

Received 23 March 2007; received in revised form 4 June 2007
Available online 23 August 2007

Abstract

The vascularization of smart materials with self-healing functionality requires the distribution of fluids continuously and uniformly throughout the material volume. This paper shows how to configure the architecture such that the single stream that flows through the vascularized body has access to every volume element. The configuration is two trees matched canopy to canopy, and has freedom to morph in several directions: channel orientations (diagonal vs. orthogonal), channel sizes, and system sizes. Tree–tree configurations provide greater access when diagonal channels are combined with orthogonal channels, and when multiple and optimized channel sizes are used.

1. Introduction

A new direction in the design of smart materials is the invention of structural composites with distributed (encapsulated) healing fluids such as epoxy [1]. When the material is overworked and it develops tiny cracks, the embedded capsules break, and the healing and curing agents fill and fuse the cracks. It was demonstrated that after a certain healing time the composite regains its mechanical strength properties.

The filling of cracks with fluid from microcapsules is a one-time healing process. The future development of self-healing composites calls for the use of *vascularization* with healing agents, so that the entire volume of the structural composite is protected against volumetric cracking. Several cracks may form randomly and at different sites simultaneously and repeatedly. One-time healing is not the solution. Needed is a network that is configured and distributed optimally through the composite so that it provides healing agent where and when self-healing is needed.

The manufacturability of such vascularization has been demonstrated [2]: three-dimensional architectures can be constructed by direct-write assembly of fugitive organic inks. The resulting grids have smooth cylindrical channels with defined connectivity and diameters in the range 30–300 μm.

The latest work on the vascularization of smart materials focuses on the fundamental problem of how to provide fluid to every point in a solid slab in which cracks may occur. The approach that was chosen is based on constructal theory [3,4], which regards the generation of flow configuration as a natural phenomenon that evolves in time toward easier flowing configurations. All flow systems in nature have configuration (i.e., geometry, architecture, drawing). Constructal theory places the occurrence of flow configuration on the basis of a physics principle (the constructal law): "For a flow system to persist in time (to survive) it must evolve in such a way that it provides easier and easier access to the currents that flow through it". The constructal law has become an addition to thermodynamics: the thermodynamics of flow systems with configu-

* Corresponding author. Tel.: +1 919 606 5314; fax: +1 919 660 8963.
E-mail address: abejan@duke.edu (A. Bejan).

0017-9310/$ - see front matter © 2007 Elsevier Ltd. All rights reserved.
doi:10.1016/j.ijheatmasstransfer.2007.06.015

Nomenclature

a	ratio, Eq. (15)
A	area, m^2
C	factor, Eq. (3)
d	elemental length scale, m
D_i	channel diameter, m
H	height of rectangular domain, m, Fig. 1
L	length rectangular domain, m, Fig. 1
L_i	channel length, m
$\dot{m}$	mass flow rate, $kg\ s^{-1}$
N	number of elemental sequences $d \times d$ in one direction
R	flow resistance, Fig. 5
Sv	svelteness number, Eq. (2)
V	total volume, m^3
V_c	total flow volume, m^3
x, y	variables, m^2, Eq. (15)

Greek symbols

ΔP	pressure difference, Pa
ν	kinematic viscosity, $m^2\ s^{-1}$
ϕ	porosity
ψ	non-dimensional global flow resistance, Eq. (14)

Subscripts

i	channel rank
c	channel
min	minimum
opt	optimum

ration [5]. The progress in this new domain was reviewed most recently in Ref. [6].

Constructal flow architectures are a fast growing body of work that has two main thrusts. One relies on the constructal law to predict and explain the occurrence of natural flow patterns in animate and inanimate systems (e.g., Refs. [6–9]). The other direction is the use of the constructal law as a scientific principle in engineering design (e.g., Refs. [10–24]). This activity of "design as science" forms the subject of this article.

Special among the engineered flow architectures derived from the constructal law are the tree-shaped (dendritic) designs. They are invading technological domains in which they were not used previously (e.g., electronics cooling, fuel cells). The reason is that because of their multiple scales and optimized (finite) complexity, tree flows offer greater densities of heat and mass transfer. Tree-shaped flow configurations offer maximum access between one point (inlet, or outlet) and an infinite number of points (area, volume). Many superimposed tree flows are accommodated by a grid of channels, which resembles the grid of city traffic.

By using two trees matched canopy to canopy, it is possible to provide healing fluid to one or more sites where cracks may develop. The crack length scale d is known and fixed. Each crack site is modeled as a sphere of diameter d. The composite material is a slab of thickness d. The tree networks must be fine enough so that they touch all the cracks wherever they may occur. The flow rate through the entire network ($\dot{m}$) is steady and much larger than the flow rate needed to fill the cracks that may form. Consequently, the flow through the network is modeled as steady and incompressible.

The new concept explored in this paper is the use of diagonal channels in architectures that consist of two trees matched canopy to canopy (Fig. 1). The self-healing composite is a slab with rectangular face: on it, the layout of the flow is two-dimensional. This architecture was originally

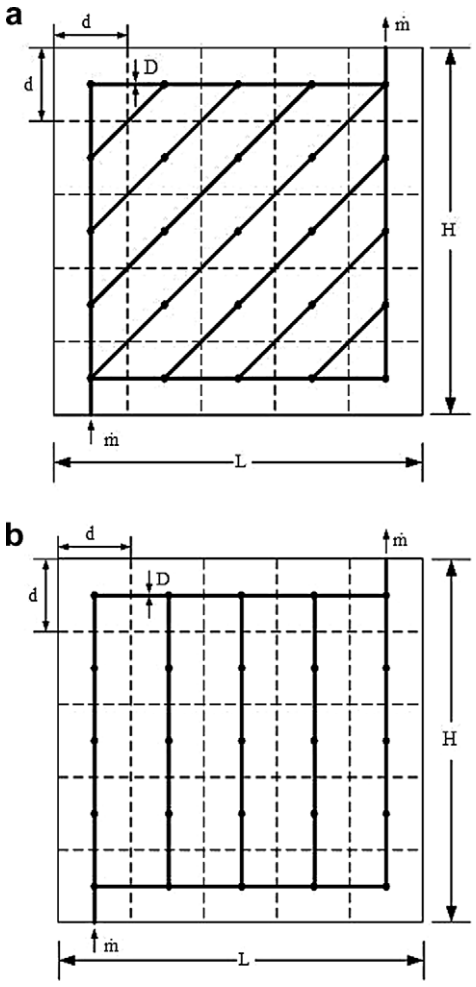

Fig. 1. Trees matched canopy to canopy on square flow domains with square elements ($d \times d$), and channels with one diameter (D): (a) diagonal channels, (b) orthogonal channels.

proposed for cooling with orthogonal channels a rectangular domain [25], and it was since adopted for the development of microscale flow structures [22,23,26].

2. Model

The modeling of the flow architectures described in this paper is based on several assumptions, which are selected such that the present results can be compared on the same basis with the results of Ref. [27], where all the channels were orthogonal. First, the volume fraction occupied by all the channels is held fixed,

$$\phi = \frac{V_c}{V} = \frac{\text{total channel volume}}{\text{total volume}} \tag{1}$$

It is further assumed that the svelteness of the network, Sv, is greater than 10,

$$Sv = \frac{(HL)^{1/2}}{V_c^{1/3}} = \frac{\text{external length scale}}{\text{internal length scale}} \tag{2}$$

As shown in Ref. [28], when Sv exceeds the order of 10, the pressure losses are dominated by Poiseuille fluid friction along the straight channels, and losses due to bends and junctions are negligible. The svelteness Sv is a global property of the flow architecture, and it plays an important role in the evolution of the flow architecture toward the best or near-best architecture (near the "equilibrium flow configuration" [5]). The assumption that $Sv > 10$ is consistent with the application of these designs to self-healing composites, where channel diameters are expected to be in the 10–100 μm range, with Reynolds numbers of order 1.

The flow in every channel is in the Poiseuille regime. The pressure drop along a channel with length L_i, diameter D_i, and mass flow rate $\dot{m}_i$ is

$$\Delta P_i = C\frac{\dot{m}_i L_i}{D_i^4} \tag{3}$$

where v is the kinematic viscosity, and C is a constant factor, for example, $C = 128v/\pi$ if the duct cross-section is round. Eq. (3) continues to be valid for other cross-sectional shapes (with slightly different values for C) provided that D_i is the hydraulic diameter of channel i, and that the shape of the channel cross-section does not change from one channel to the next. For example, if all the channels have square cross-sections, then $C = 12v$.

We used this model in order to simulate flows in a large number of configurations of channels, so that we were able to optimize the configurations. The objective was to uncover trends and to devise *strategies* that can be used in future designs of tree-shaped vascularization. The work was conducted systematically by focusing on the major features of the design: diagonal vs. orthogonal channels, one channel diameter vs. two or three channel diameters, combined diagonal and orthogonal channels, and the effect of changing the size and shape of the two-dimensional domain occupied by the vascularization.

3. Diagonal and orthogonal channels with one diameter

Consider the square domain composed of 5 × 5 elemental squares in Fig. 1. Two types of trees matched canopy-to-canopy are shown: (a) two trees with diagonal channels and two peripheral orthogonal channels, and (b) two trees with only orthogonal channels. Both types satisfy the key requirement of vascularization of self-healing and self-cooling, which is that the center of every elemental square must be touched by at least one channel. This guarantees that all the potential crack sites of length scale d have access to healing fluid.

We illustrate the analysis by applying it to the simplest case, which is shown in Fig. 2. There are only 3 × 3 elemental squares. For Fig. 2a, we calculate the total pressure

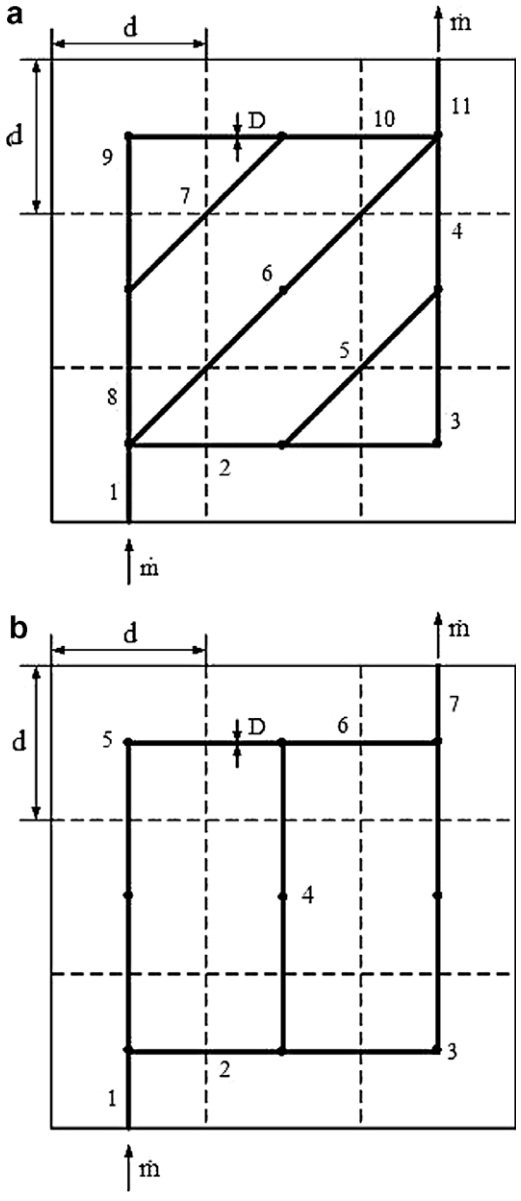

Fig. 2. Square domain with 3 × 3 elemental squares and channels with one diameter.

Table 1
Optimized designs with orthogonal and diagonal channels when the channels have only one diameter size

$N \times N$	$\frac{\Delta P}{Cd\dot{m}}\left(\frac{V_c}{d}\right)^2$		$\frac{\Delta P_b - \Delta P_a}{\Delta P_b}$	$\frac{\Delta P}{C\dot{m}}\phi^2 d^3$	
	Diagonal channels	Orthogonal channels		Diagonal channels	Orthogonal channels
3 × 3	257.19	205.87	−0.249	3.175	2.542
4 × 4	904.43	765.45	−0.182	3.533	2.990
5 × 5	2368.7	2125.3	−0.115	3.789	3.400
6 × 6	5186.9	4914.5	−0.055	4.002	3.792
7 × 7	10,060	10,022	−0.004	4.189	4.174
8 × 8	17,866	18,621	−0.041	4.362	4.546
9 × 9	29,671	32,313	−0.082	4.522	4.925
10 × 10	46,743	53,233	−0.122	4.674	5.323

drop across the entire flow structure by writing

$$\Delta P = \Delta P_1 + \Delta P_6 + \Delta P_{11} = C\left(\frac{\dot{m}_1 d/2}{D^4} + \frac{\dot{m}_6 2^{3/2} d}{D^4} + \frac{\dot{m}_{11} d/2}{D^4}\right) \quad (4)$$

The continuity of mass requires

$$\begin{aligned} &\dot{m} = \dot{m}_1 = \dot{m}_2 + \dot{m}_6 + \dot{m}_8 = \dot{m}_4 + \dot{m}_6 + \dot{m}_{10} = \dot{m}_{11} \\ &\dot{m}_2 = \dot{m}_3 + \dot{m}_5 = \dot{m}_4 \\ &\dot{m}_8 = \dot{m}_7 + \dot{m}_9 = \dot{m}_{10} \end{aligned} \quad (5)$$

Because of symmetry, we also have

$$\Delta P_6 = \Delta P_2 + \Delta P_3 + \Delta P_4 = \Delta P_2 + \Delta P_5 + \Delta P_4 = \Delta P_8 + \Delta P_7 + \Delta P_{10} = \Delta P_8 + \Delta P_9 + \Delta P_{10} \quad (6)$$

The total channel volume constraint reads

$$V_c = \frac{\pi}{4} D^2 (9 + 2^{5/2}) d \quad (7)$$

Combining Eqs. (4)–(7) we find that the total pressure drop can be expressed non-dimensionally as

$$\frac{\Delta P}{Cd\dot{m}}\left(\frac{V_c}{d}\right)^2 = 257.19 \quad (8)$$

The corresponding analysis of the 3 × 3 orthogonal configuration of Fig. 2b yields, in order,

$$\Delta P = \Delta P_1 + \Delta P_2 + \Delta P_3 + \Delta P_7 = C\left(\frac{\dot{m}_1 d/2}{D^4} + \frac{\dot{m}_2 d}{D^4} + \frac{\dot{m}_3 3d}{D^4} + \frac{\dot{m}_7 d/2}{D^4}\right) \quad (9)$$

$$\begin{aligned} &\dot{m} = \dot{m}_1 = \dot{m}_2 + \dot{m}_5 = \dot{m}_3 + \dot{m}_6 = \dot{m}_7 \\ &\dot{m}_2 = \dot{m}_3 + \dot{m}_4 \\ &\dot{m}_6 = \dot{m}_4 + \dot{m}_5 \end{aligned} \quad (10)$$

$$\Delta P_2 + \Delta P_3 = \Delta P_2 + \Delta P_4 + \Delta P_6 = \Delta P_5 + \Delta P_6 \quad (11)$$

$$V_c = \frac{\pi}{4} D^2 \left(\frac{1}{2} \cdot 2 + 1 \cdot 4 + 2 \cdot 3\right) d \quad (12)$$

$$\frac{\Delta P}{Cd\dot{m}}\left(\frac{V_c}{d}\right)^2 = 205.87 \quad (13)$$

By comparing Eqs. (8) and (13), we see that the design of Fig. 2b is superior to that of Fig. 2a, because its global flow resistance is smaller by 24.9%. But in Table 1 the relative difference of global flow resistance between the two designs gradually decreases as the system size increases so that for $N > 7$ the values of these resistances are reversed. This is a promising result, which we pursued in greater detail in Section 4. However, it is important to note that although both designs (Fig. 2a and b) satisfy the requirement that channels must pass through the centers of all the elemental squares, in Fig. 2a the triangular and trapezoidal loops

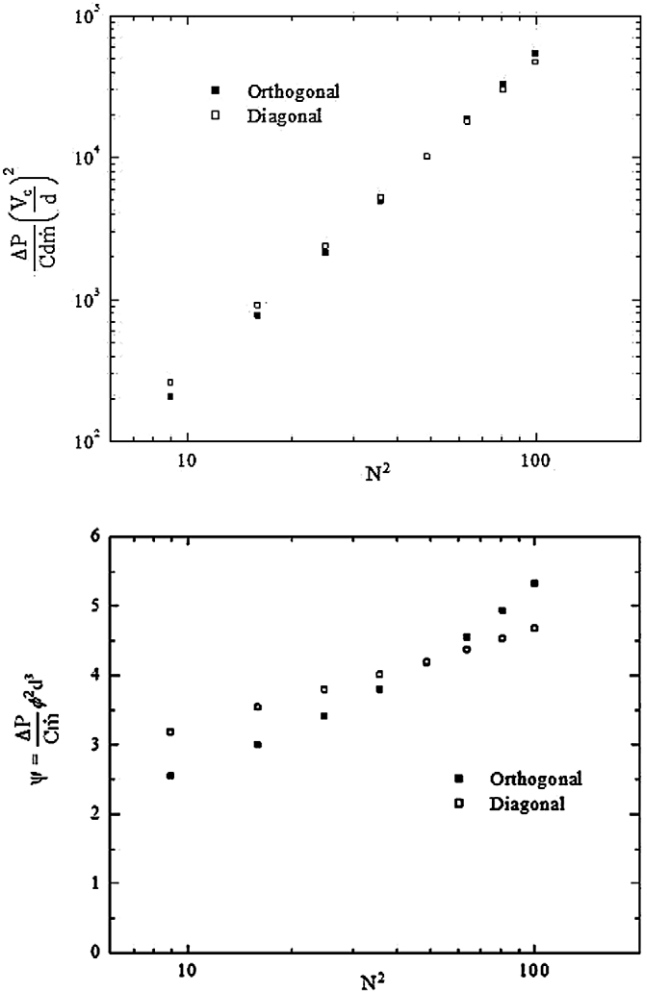

Fig. 3. The global flow resistances of the flow architectures shown in Fig. 1a and b.

are narrower than the loops visible in Fig. 2b. This means that the circles inscribed in the loops of Fig. 2a have a diameter that is smaller than the diameter (d) of the circle inscribed in the rectangular loop of Fig. 2b. Said another way, the loops of Fig. 2a are over designed.

In Table 1, we show the results for the architecture of Fig. 1 on square domains $N \times N$ that increase in size all the way to 10×10. The orthogonal design (b) is better than the diagonal design (a) when $N \leqslant 7$. Above $N = 7$, the diagonal design is better. The relative difference between the two is in the range of 25%. The data of Table 1 are plotted in Fig. 3, which shows the effect of global size: the overall pressure drop increases roughly in proportion to $N^{4.32}$ and $N^{4.61}$ for design (a) and design (b), respectively.

Another way to non-dimensionalize the overall pressure drop (by accounting for the $N \times N$ system size in the non-dimensional group) is by constructing the group

$$\psi = \frac{\Delta P}{C\dot{m}}\phi^2 d^3 \tag{14}$$

This alternative group is calculated on the right side of Table 1, and plotted in the lower part of Fig. 3. Both ΔP groups increase as the system size (N^2) increases.

4. Channels with two diameters

Earlier constructal design studies [5,27] showed that one strategy for improved global flow performance is to endow the flow architecture with more freedom (for example, more than one channel diameter), and to optimize the ratio of the diameters of the channels that meet at a junction. This opportunity for achieving better performance is well known in the vascularization of living tissues, cf. the Hess–Murray law [29,30] and the tree architectures derived based on the constructal law.

In Fig. 4, we show the simplest example of how to install channels with two diameters in a tree–tree structure that covers a square domain with 4×4 elements. We know from earlier work in constructal theory [3,4] that the thinner channels (D_1) should be placed in the canopy, and the thicker (D_2) in the stem and main branches. There are two

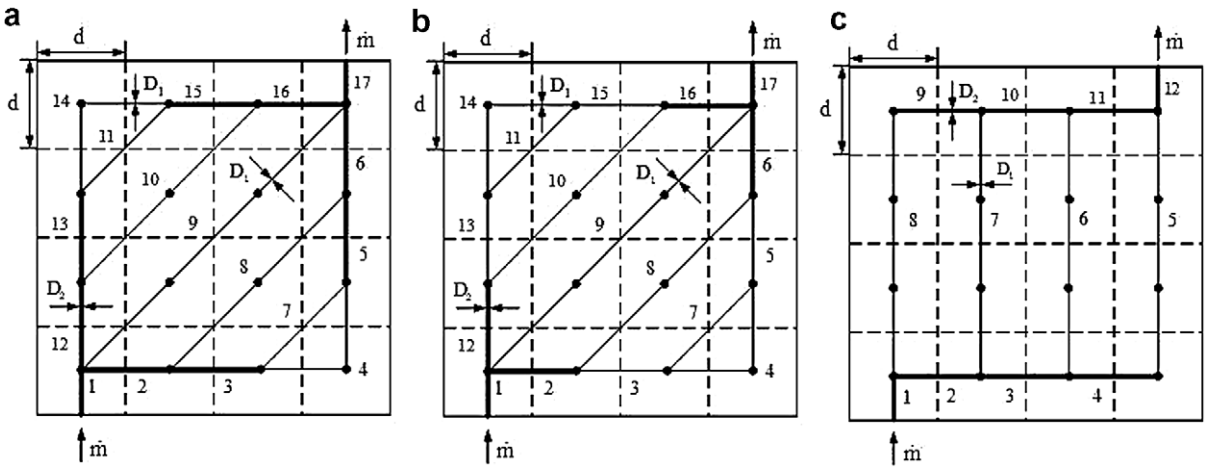

Fig. 4. Square flow domains with channels with two sizes (D_1, D_2): (a) diagonal channels, (b) diagonal channels, (c) orthogonal channels.

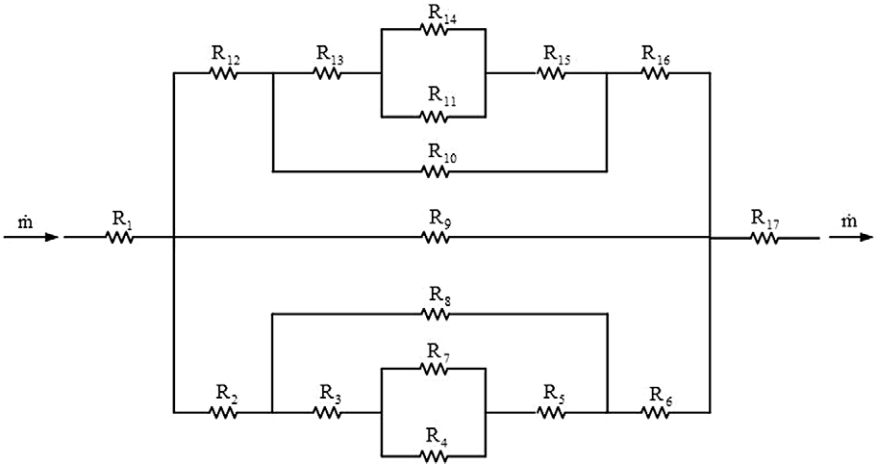

Fig. 5. The equivalent flow resistance of the configuration shown in Fig. 4a.

Table 2
Optimal designs of diagonal and orthogonal channels with two diameter size

$N \times N$	$\left(\frac{D_1}{D_2}\right)_{opt}$			$\left[\frac{\Delta P}{\dot{C}\dot{m}}\left(\frac{V_c}{d}\right)^2\right]_{min}$			$\left(\frac{\Delta P}{\dot{C}\dot{m}}\phi^2 d^3\right)_{min}$		
	Diagonal channels (Fig. 4a)	Diagonal channels (Fig. 4b)	Orthogonal channels	Diagonal channels (Fig. 4a)	Diagonal channels (Fig. 4b)	Orthogonal channels	Diagonal channels (Fig. 4a)	Diagonal channels (Fig. 4b)	Orthogonal channels
3 × 3	0.699	0.640	0.803	187.53	177.36	179.57	2.315	2.189	2.217
4 × 4	0.656	0.667	0.739	624.79	594.34	594.00	2.441	2.322	2.321
5 × 5	0.616	0.638	0.691	1525.3	1464.2	1460.2	2.440	2.343	2.336
6 × 6	0.580	0.608	0.653	3102.6	3012.6	3004.2	2.394	2.325	2.318
7 × 7	0.549	0.579	0.621	5595.2	5492.3	5488.6	2.330	2.288	2.286
8 × 8	0.524	0.554	0.595	9263.4	9181.3	9201.5	2.262	2.242	2.246
9 × 9	0.501	0.531	0.573	14,387	14,381	14,486	2.193	2.192	2.208
10 × 10	0.481	0.511	0.554	21,266	21,413	21,701	2.127	2.141	2.170

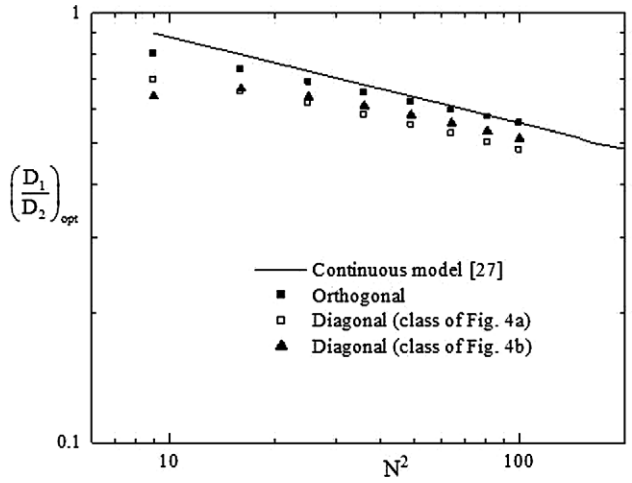

Fig. 6. The optimal ratio of channel diameters for the diagonal vs. orthogonal tree–tree configurations optimized in Table 2.

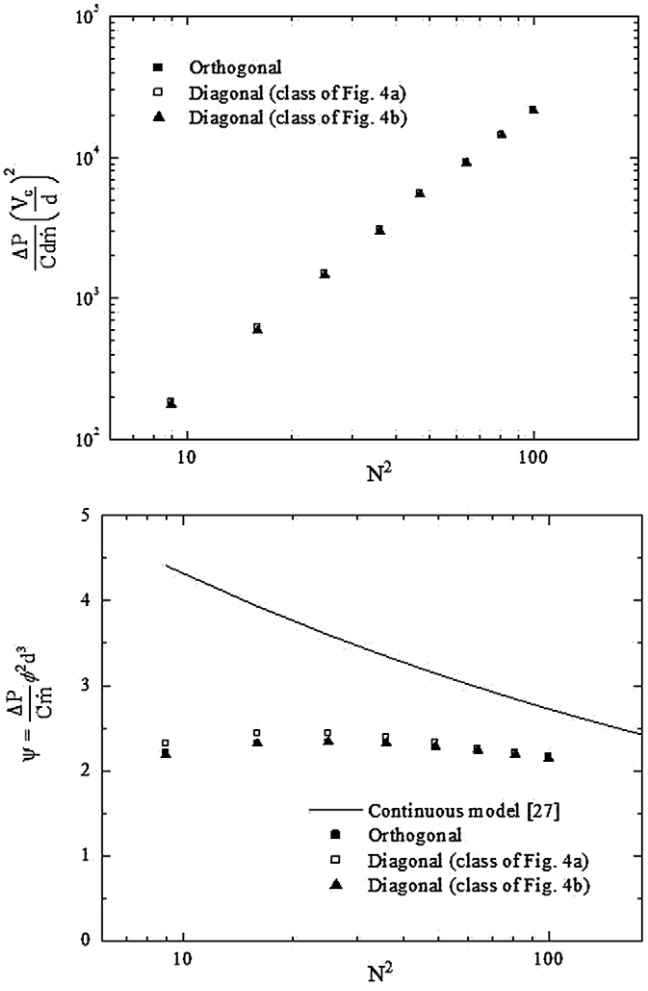

Fig. 7. The minimized global flow resistance for the diagonal vs. orthogonal tree–tree configurations optimized in Table 2.

types of diagonal designs having two channel sizes in Fig. 4. They differ with respect to how we place the thinner channels (D_1) or the thicker channels (D_2) on the trapezoidal loops, which are linked with the triangular loops.

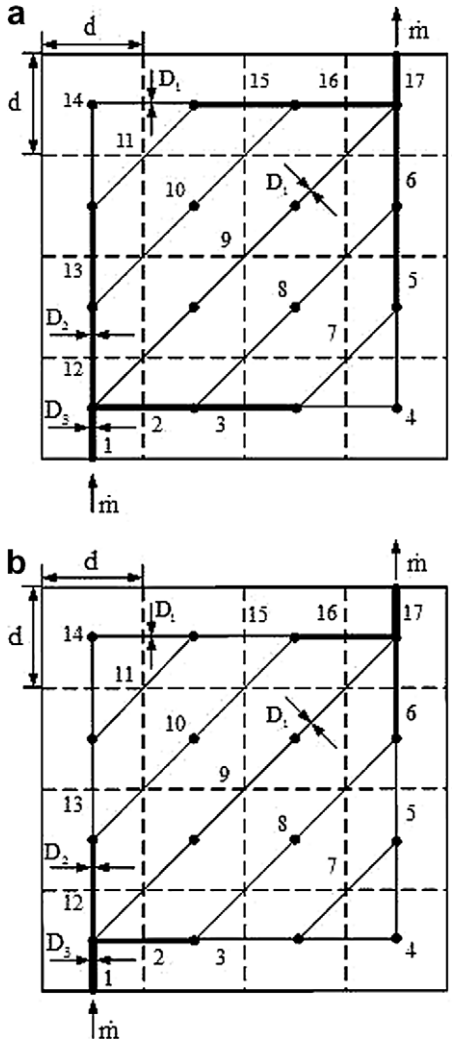

Fig. 8. Tree–tree configurations with diagonal channels with three sizes (D_1, D_2, D_3): (a) diagonal channels and (b) diagonal channels.

The diagonal design (Fig. 4a) was optimized by using the method presented in Section 3. For every channel we write the Poiseuille flow relation, Eq. (3), which shows that the local flow resistance $\Delta P/\dot{m}_i$ is proportional to the geometric ratio L_i/D_i^4. For the sake of brevity, in the following analysis we use only L_i/D_i^4 for flow resistance, instead of the full expression of Eq. (3). Fig. 5 shows the equivalent flow resistance network corresponding to the configuration of Fig. 4a. Next, we use the notation

$$D_1^2 = x, \quad D_2^2 = y, \quad a = \frac{x}{y} \tag{15}$$

The R_4 and R_7 resistances are in parallel and their combined resistance R_{47} is

$$R_{47} = x^{-2}(2^{-1} + 2^{-1/2})^{-1} d \tag{16}$$

The combined resistance of R_3, R_{47} and R_5 is $R_{3-47-5} = R_3 + R_{47} + R_5$. This can be expressed in terms of x and a:

$$R_{3-47-5} = \frac{d}{x^2}\left(2a^2 + \frac{1}{2^{-1} + 2^{-1/2}}\right) = R_{3B} = \frac{d}{x^2} R_{3BB} \tag{17}$$

Here, R_{3B} is shorthand for R_{3-47-5}, and R_{3BB} is shorthand for the quantity inside brackets in Eq. (17). The equivalent resistance of R_{3B}, R_8, R_2, R_6 is

$$R_{3B-8-2-6} = \frac{d}{x^2}\left(2a^2 + \frac{1}{R_{3BB}^{-1} + 2^{-3/2}}\right) = R_{4B} = \frac{d}{x^2} R_{4BB} \tag{18}$$

Here, R_{4B} is shorthand for $R_{3B-8-2-6}$, and R_{4BB} is shorthand for the quantity inside brackets in Eq. (18). The total resistance of the tree–tree network is

$$\begin{aligned} R_{t,4} &= R_1 + \left(\frac{2}{R_{4B}} + \frac{1}{R_9}\right)^{-1} + R_{17} \\ &= \frac{d}{x^2}\left[a^2 + \left(\frac{2}{R_{4BB}} + \frac{1}{3 \cdot 2^{1/2}}\right)^{-1}\right] \end{aligned} \tag{19}$$

The total channel volume constraint is

$$V_c = \frac{\pi}{4} d\left[(4 + 9 \cdot 2^{1/2})x + 9y\right] \tag{20}$$

or, in terms of x and a,

$$\left(\frac{V_c}{d}\right)^2 = \left(\frac{\pi}{4}\right)^2 \left[(4 + 9 \cdot 2^{1/2}) + 9/a\right]^2 x^2 \tag{21}$$

By combining Eqs. (19) and (21), we find the global flow resistance

$$\frac{\Delta P}{C\dot{m}}\left(\frac{V_c}{d}\right)^2 = \left(\frac{\pi}{4}\right)^2 \left[a^2 + \left(\frac{2}{R_{4BB}} + \frac{1}{3 \cdot 2^{1/2}}\right)^{-1}\right] \left[(4 + 9 \cdot 2^{1/2}) + 9/a\right]^2 \tag{22}$$

Table 3
The optimal designs for trees with two and three channel sizes, based on Figs. 4a and 8a

$N \times N$	Two diameters		Three diameters			$\frac{\Delta P_2 - \Delta P_3}{\Delta P_2}$
	$\left(\frac{D_1}{D_2}\right)_{opt}$	$\left(\frac{\Delta P_2}{C\dot{m}}\phi^2 d^3\right)_{min}$	$\left(\frac{D_1}{D_2}\right)_{opt}$	$\left(\frac{D_1}{D_3}\right)_{opt}$	$\left(\frac{\Delta P_3}{C\dot{m}}\phi^2 d^3\right)_{min}$	
3×3	0.699	2.315	0.806	0.587	2.036	0.121
4×4	0.656	2.441	0.736	0.523	2.151	0.119
5×5	0.616	2.440	0.676	0.477	2.186	0.104
6×6	0.580	2.394	0.627	0.442	2.179	0.089
7×7	0.549	2.330	0.587	0.414	2.149	0.078
8×8	0.524	2.262	0.554	0.391	2.109	0.068
9×9	0.501	2.193	0.526	0.372	2.063	0.059
10×10	0.481	2.127	0.503	0.355	2.015	0.053

Table 4
The optimal designs for trees with two and three channel sizes, based on Figs. 4b and 8b

$N \times N$	Two diameters		Three diameters			$\frac{\Delta P_2 - \Delta P_3}{\Delta P_2}$
	$\left(\frac{D_1}{D_2}\right)_{opt}$	$\left(\frac{\Delta P_2}{C\dot{m}}\phi^2 d^3\right)_{min}$	$\left(\frac{D_1}{D_2}\right)_{opt}$	$\left(\frac{D_1}{D_3}\right)_{opt}$	$\left(\frac{\Delta P_3}{C\dot{m}}\phi^2 d^3\right)_{min}$	
3×3	0.640	2.189				
4×4	0.667	2.322	0.755	0.557	2.139	0.079
5×5	0.638	2.343	0.703	0.505	2.138	0.087
6×6	0.608	2.325	0.659	0.467	2.132	0.083
7×7	0.579	2.288	0.621	0.437	2.115	0.076
8×8	0.554	2.242	0.588	0.413	2.089	0.068
9×9	0.531	2.192	0.560	0.393	2.058	0.061
10×10	0.511	2.141	0.536	0.376	2.024	0.055

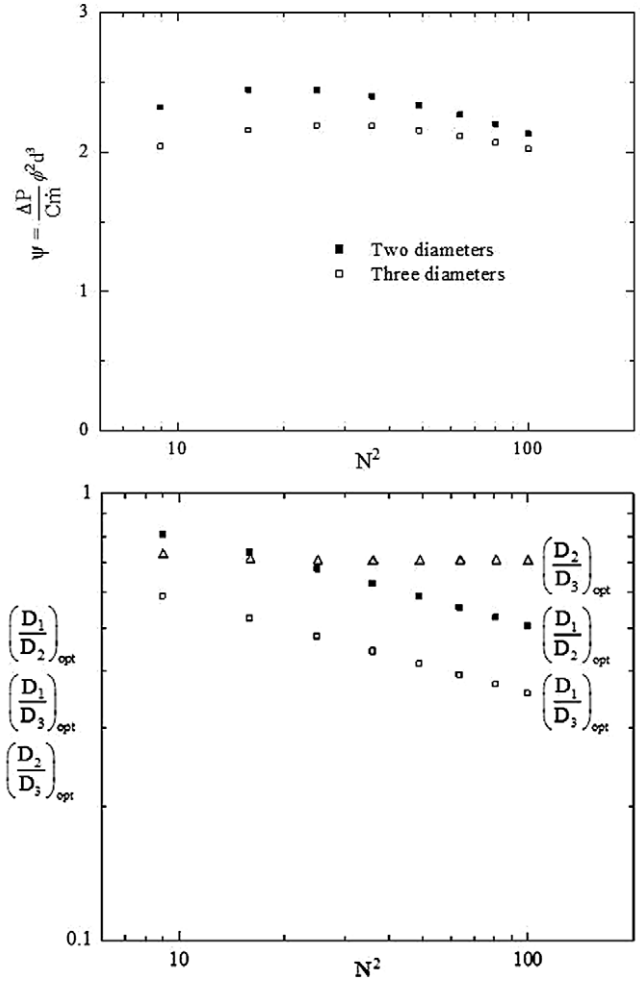

Fig. 9. The minimized flow resistance and optimized ratios of channel sizes for the configurations shown in Fig. 8a and Table 3.

By minimizing this expression with respect to a, we obtain the optimal ratio of diameters and the minimized flow resistance

$$\left(\frac{D_1}{D_2}\right)_{opt} = 0.656 \tag{23}$$

$$\frac{\Delta P}{Cd\dot{m}}\left(\frac{V_c}{d}\right)^2 = 624.79 \tag{24}$$

These results are reported in Table 2, which shows the minimized global ΔP and optimal D_1/D_2 for the diagonal and orthogonal configurations defined in Fig. 4. The overall system size increases from 3×3 to 10×10. The optimal ratio D_1/D_2 is shown in Fig. 6. The diagonal and orthogo-

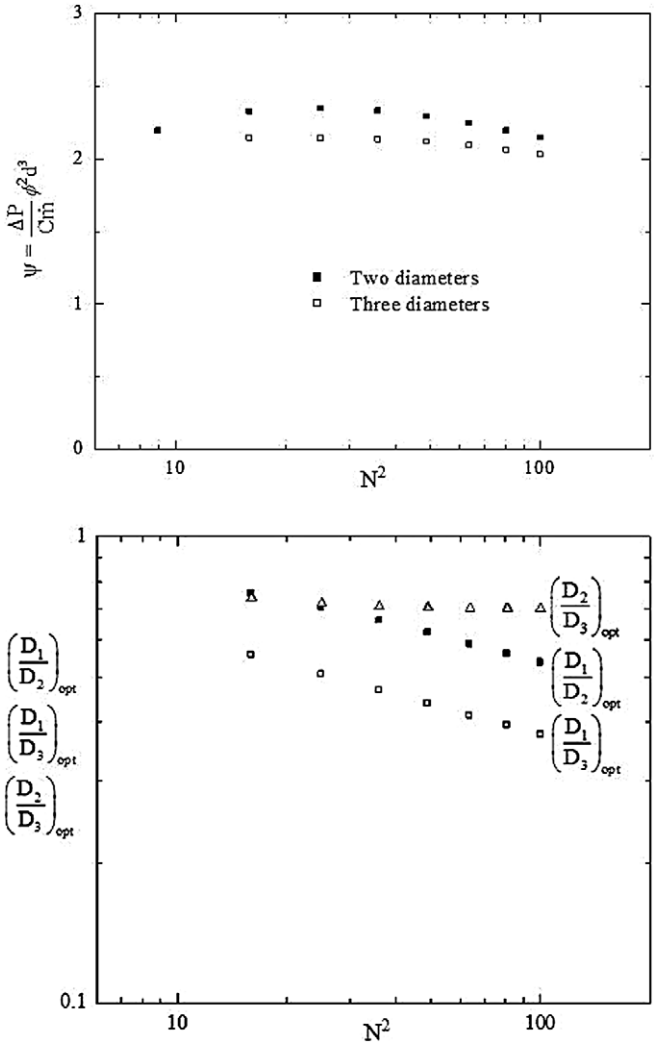

Fig. 10. The minimized flow resistance and optimized ratios of channel sizes for the configurations shown in Fig. 8b and Table 4.

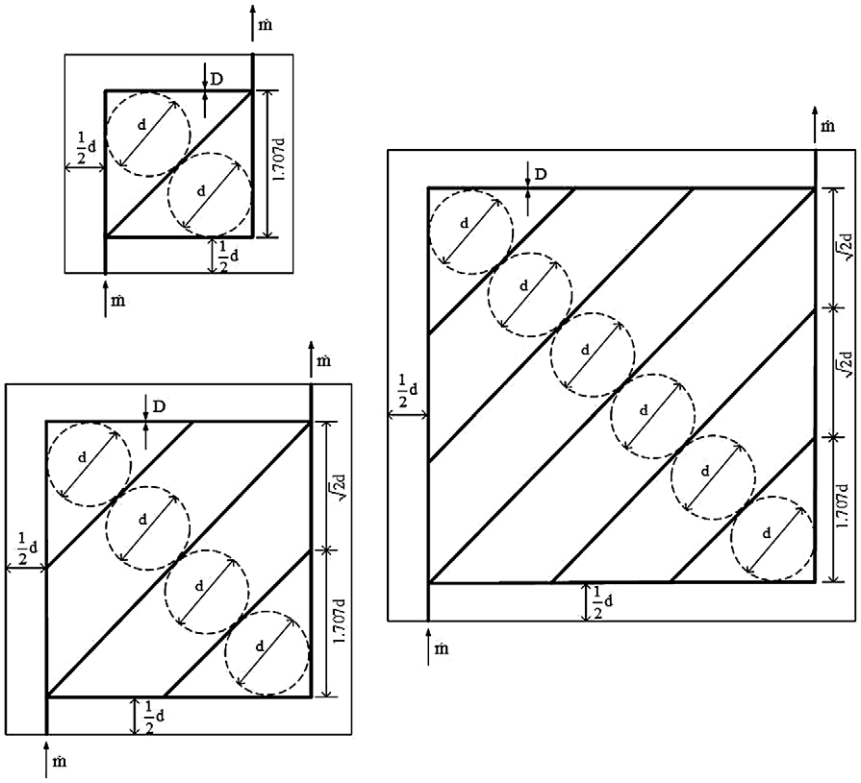

Fig. 11. Trees matched canopy to canopy with diagonal channels of one size, and loops (inscribed circles) of one size.

Table 5
Designs with diagonal channels having the same inscribed circle (d), and one channel size (D)

$H = L$	$\frac{\Delta P}{C\dot{m}}\left(\frac{V_c}{d}\right)^2$	$\frac{\Delta P}{C\dot{m}}\phi^2 d^3$
2.707d	129.28	2.408
4.121d	774.32	2.684
5.535d	2649.9	2.822
6.949d	6831.7	2.929
8.364d	14803	3.025
9.778d	28497	3.117
11.19d	50327	3.207
12.61d	83224	3.295

nal designs have nearly the same $(D_1/D_2)_{\text{opt}}$ values, which decrease in the same manner as the grid size increases.

Fig. 7 shows the corresponding minimized global resistance vs. the size of the square domain $N \times N$. The upper graph shows the overall flow resistance reported as the group $(\Delta P/C d\dot{m})(V_c/d)^2$. The lower graph shows the corresponding ΔP results reported as $\psi = (\Delta P/C\dot{m})\phi^2 d^3$. Both presentations suggest that diagonal designs and orthogonal design perform in nearly the same way. Systems larger than 7×7 are bathed almost as effectively by both designs.

Note the agreement between the present numerical results and the analytical solution developed for orthogonal channels with $N \gg 1$ in Ref. [27]. The analytical solution is indicated with solid line in Figs. 6 and 7. It serves as asymptote for the numerical results for grids with orthogonal channels, and anticipates closely the trend for optimized grids with diagonal channels.

Table 6
The optimal designs having the same inscribed (d) for trees with two and three channel sizes

$H = L$	Two diameters		Three diameters			$\frac{\Delta P_2 - \Delta P_3}{\Delta P_2}$
	$\left(\frac{D_1}{D_2}\right)_{\text{opt}}$	$\left(\frac{\Delta P_2}{C\dot{m}}\phi^2 d^3\right)_{\min}$	$\left(\frac{D_1}{D_2}\right)_{\text{opt}}$	$\left(\frac{D_1}{D_3}\right)_{\text{opt}}$	$\left(\frac{\Delta P_3}{C\dot{m}}\phi^2 d^3\right)_{\min}$	
2.707d	0.690	1.811				
4.121d	0.717	2.037	0.805	0.586	1.842	0.096
5.535d	0.674	2.022	0.736	0.523	1.835	0.092
6.949d	0.632	1.959	0.679	0.478	1.802	0.080
8.364d	0.595	1.886	0.632	0.444	1.757	0.068
9.778d	0.564	1.814	0.593	0.416	1.707	0.059
11.19d	0.537	1.744	0.561	0.394	1.656	0.050
12.61d	0.514	1.680	0.533	0.375	1.605	0.045

5. Channels with three diameters

The next step in the direction of more design freedom (hence higher global performance [5]) is to permit the channels to have three channel sizes, not two. The channel sizes (D_1, D_2, D_3) are indicated in Fig. 8 for grids with 4×4 elements. The difference between the channel arrangements is the same as in Fig. 4a and b. To distribute the flow volume optimally to these channels means to optimize two ratios, D_1/D_2 and D_1/D_3. We performed this work for grids that increase in size from 3×3 to 10×10. The method is the same as in the preceding section, therefore the analytical details omitted. Note that the 3×3 diagonal configuration of the type shown in Fig. 8b cannot be constructed with three different diameters.

The results are shown on the right side of Tables 3 and 4 by using the group $\psi = (\Delta P/C\dot{m})\phi^2 d^3$. They indicate the optimal distribution of channel sizes and the minimized pressure drop. The left sides of the tables show the corresponding designs and performance of trees with two channel sizes, which were seen in Table 2. The comparison of the two classes of designs shows that the switch from two to three channels sizes induces a reduction of 5–12% in the overall flow resistance of the tree-to-tree construct.

This reduction is presented graphically in Figs. 9 and 10. The reduction decreases gradually as N increases. Figs. 9 and 10 also show the behavior of the optimized channel size ratios (D_1/D_2, D_1/D_3) as the system size increases. The two ratios decrease at almost the same rate as N^2 increases, meaning that the third ratio that can be formed with the three sizes (D_2/D_3) is nearly insensitive to N. Indeed, the data of Tables 3 and 4 show that D_2/D_3 takes values in the narrow range 0.73–0.7 when N increases from 3 to 10.

6. Loops with one size

In Fig. 1a, we saw that when diagonal channels pass through the centers of the $d \times d$ square elements, the loops are narrower than the spacing required by one crack length scale (d). In this section we repeat the configurations and performance of diagonal configurations that have the loop width (d) distributed throughout the network. In other words, we give the configuration of Fig. 1a more freedom to morph, so that the channels are arranged as in Fig. 11.

In these new configurations, every loop is such that the largest circle that can be inscribed in the loop has the crack site diameter d.

In Fig. 11, we illustrate this new class of tree–tree configurations for three cases. The size of the inscribed circle (d) does not vary as the system size increases. The margin left around the vascularized area of the slab has the width $d/2$.

To make the comparison between the designs of Figs. 11 and 1a possible, in Fig. 11 we used channels with a single diameter (D). The analytical method for calculating the global ΔP for the configurations of Fig. 11 is the same as in Section 3. The results are summarized in Table 5. The corresponding results for the original diagonal designs (Fig. 1a) are listed in Table 1. As noted above, the comparison cannot be made with the previous designs because the size of the $N \times N$ slab in Fig. 1a is not exactly the same as the size of a comparable slab in Fig. 11.

This is why in Fig. 13 we plotted on the abscissa the total area of the square slab (A), divided by the constant d^2. For example, the 3×3 slab of Fig. 2a is represented by $A/d^2 = 9$ on the abscissa of Fig. 13, whereas the corresponding comparable slab of Fig. 11 (the lower left diagonal configuration with four inscribed circles) is represented by $A/d^2 = 16.98$.

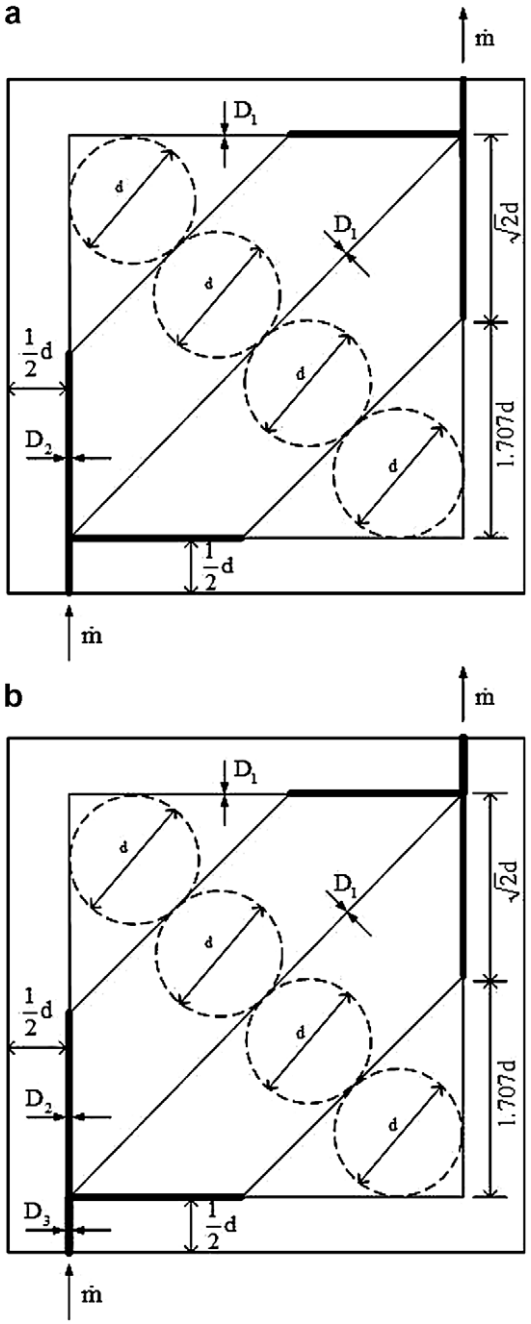

Fig. 12. Trees matched canopy to canopy with diagonal channels of multiple sizes, and loops (inscribed circles) of one size: (a) two diameters (D_1, D_2), (b) three diameters (D_1, D_2, D_3).

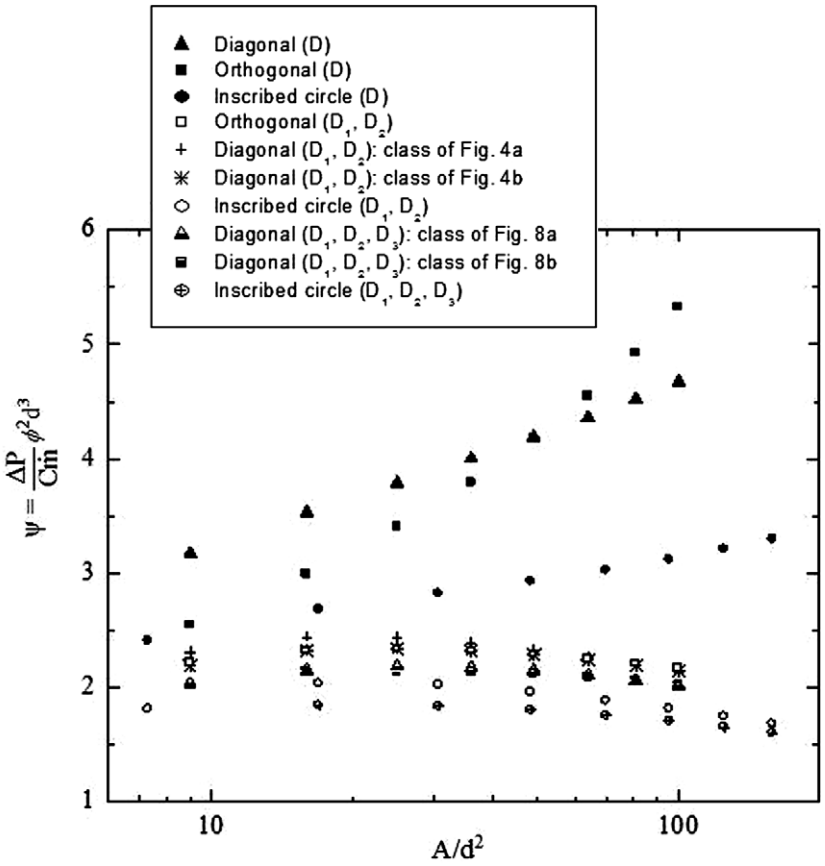

Fig. 13. Summary of the global flow resistances of all the tree–tree designs developed in this paper.

Next, we increased the freedom to morph the channel sizes. In Table 6, we report the results of the optimal designs having loops with one size (d) for trees with two and three diameters. Fig. 12 shows two configurations with four inscribed circles. The overall system size increases from two inscribed circles ($H = L = 2.707d$) to 16 inscribed circles ($H = L = 12.61d$). The analytical method is the same as in Sections 4 and 5.

Fig. 13 shows how the dimensionless flow resistance $\psi = (\Delta P/C\dot{m})\phi^2 d^3$ varies with the system size A/d^2 in all the architectures presented in our paper. We see that when the system size increases, the change in the flow architecture from Figs. 1a–11 results in a reduction of 22–33% in the global flow resistance and also the difference between the two designs increases.

Table 6 and Fig. 13 show a better performance for flow access compared with the designs of Fig. 11. The designs with three diameters are superior to the designs with two diameters. The relative difference decreases as the overall system size increases. The optimal ratios of diameters $(D_1/D_2)_{opt}$ for the designs with two diameters (Fig. 12a) have values between the values of $(D_1/D_2)_{opt}$ and $(D_1/D_3)_{opt}$ for the designs with three diameters (Fig. 12b). Furthermore, the third ratio $(D_2/D_3)_{opt}$ is practically insensitive to the system sizes. Table 6 shows that $(D_2/D_3)_{opt}$ takes values in the narrow range 0.73–0.7 (as in Section 5) as the overall system size increases.

7. Conclusions

In this paper, we studied systematically the effect that the freedom to morph the architecture has on the performance of trees matched canopy to canopy for the vascularization of smart materials with self-healing functionality. Each tree–tree architecture bathes the material body volumetrically. The search for better flow configurations is based on giving the flow system freedom to morph in several directions: channel orientations (diagonal vs. orthogonal), channel sizes (one, two, or three), and system sizes ranging from 3×3 to 10×10 elemental volumes.

We reported optimal architectures for every class. We showed that tree–tree configurations provide greater access when diagonal channels are combined with orthogonal channels, and when there are multiple and optimized channel sizes. Figs. 6, 9, 10 and 13 summarize the results for global flow resistances and channels sizes for all the designs developed in this paper. Better flow access is achieved with multiple and optimized channel sizes. For designs with more than one channel size, the relative difference between competing configurations decreases when the overall system size increases.

Section 6 described an even more efficient channel arrangement, where the loops of the network can catch all the crack sites of size d. In this class, the diagonal architectures have the same loop width (d), and are compactly arranged but not over designed.

Related to these conclusions is the work described in Ref. [31], where it was shown that an orthogonal tree with several (and optimized) channel sizes performs better than an orthogonal-with-loops design for collecting or supplying flow to an area, i.e., that the non-uniform structure provides greater overall flow access.

Acknowledgements

This research was supported by the Air Force Office of Scientific Research based on a MURI grant for the development of "Micro-Vascular Autonomic Composites" (University of Illinois at Urbana Champaign, Duke University, and University of California, Los Angeles), and based on a Grant for "Constructal Technology for Thermal Management of Aircraft". We thank Dr. David Moorhouse (Air Force Research Laboratory) for the advice and guidance that he gives us in this research direction. Jaedal Lee's work at Duke University was sponsored by the Korea Research Foundation Grant funded by the Korean Government (MOEHRD) (KRF-2006-612- D00011).

References

[1] S.R. White, N.R. Sottos, J. Moore, P. Geubelle, M. Kessler, E. Brown, S. Suresh, S. Viswanathan, Autonomic healing of polymer composites, Nature (London) 409 (2001) 794–797.
[2] D. Therriault, S.R. White, J.A. Lewis, Chaotic mixing in three-dimensional microvascular networks fabricated by direct-write assembly, Nature Mater. 2 (2003) 265–271.
[3] A. Bejan, Advanced Engineering Thermodynamics, second ed., Wiley, New York, 1997.
[4] A. Bejan, Shape and Structure: From Engineering to Nature, Cambridge University Press, Cambridge, UK, 2000.
[5] A. Bejan, S. Lorente, The constructal law and the thermodynamics of flow systems with configuration, Int. J. Heat Mass Transfer 47 (2004) 3203–3214.
[6] A. Bejan, S. Lorente, Constructal theory of generation of configuration in nature and engineering, J. Appl. Phys. 100 (2006) 041301.
[7] A. Bejan, The constructal law of organization in nature: tree-shaped flows and body size, J. Exp. Biol. 208 (2005) 1677–1686.
[8] A.K. Pramanick, P.K. Das, Note on constructal theory of organization in nature, Int. J. Heat Mass Transfer 48 (2005) 1974–1981.
[9] A.H. Reis, A.F. Miguel, M. Aydin, Constructal theory of flow architecture of the lungs, Med. Phys. 31 (2004) 1135–1140.
[10] A. Bejan, I. Dincer, S. Lorente, A.F. Miguel, A.H. Reis, Porous and Complex Flow Structures in Modern Technologies, Springer, New York, 2004.
[11] G. Hernandez, J.K. Allen, F. Mistree, Platform design for customizable products as a problem of access in a geometric space, Eng. Optimiz. 35 (2003) 229–254.
[12] H. Brod, Residence time optimized choice of tube diameters and slit heights in distribution systems for non-Newtonian liquids, J. Non-Newtonian Fluid Mech. 111 (2003) 107–125.
[13] D. Tondeur, L. Luo, Design and scaling laws of ramified fluid distributors by the constructal approach, Chem. Eng. Sci. 59 (2004) 1799–1813.
[14] Y. Chen, P. Cheng, An experimental investigation on the thermal efficiency of fractal tree-like microchannel nets, Int. Commun. Heat Mass Transfer 32 (2005) 931–938.
[15] A.Y. Alharbi, D.V. Pence, R.N. Cullion, Fluid flow through microscale fractal-like branching channel networks, J. Fluids Eng. 125 (2003) 1051–1057.
[16] A.D. Kraus, Constructal theory and the optimization of fin arrays, in: ASME International Mechanical Engineering Congress and Exposition, Washington, DC, 16–21 November, 2003.
[17] G.F. Jones, S. Ghassemi, Thermal optimization of a composite heat spreader, in: ASME Heat Transfer/Fluids Engineering Summer Conference, Charlotte, NC, 11–15 July, 2004.
[18] S.M. Senn, D. Poulikakos, Laminar mixing, heat transfer and pressure drop in tree-like microchannel nets and their application for thermal management in polymer electrolyte fuel cells, J. Power Sources 130 (2004) 178–191.
[19] S.M. Senn, D. Poulikakos, Tree network channels as fluid distributors constructing double-staircase polymer electrolyte fuel cells, J. Appl. Phys. 96 (2004) 842–852.
[20] Y. Azoumah, N. Mazet, P. Neveu, Constructal network for heat and mass transfer in a solid–gas reactive porous medium, Int. J. Heat Mass Transfer 47 (2004) 2961–2970.
[21] Y.S. Muzychka, Constructal design of forced convection cooled microchannel heat sinks and heat exchangers, Int. J. Heat Mass Transfer 48 (2005) 3119–3127.
[22] F. Lundell, B. Thonon, J.A. Gruss, Constructal networks for efficient cooling/heating, in: Second Conference on Microchannels and Minichannels, Rochester, NY, 2004.
[23] M. Lallemand, F. Ayela, M. Favre-Marinet, A. Gruss, D. Maillet, P. Marty, H. Peerhossaini, L. Tadrist, Transferts thermiques dans des microcanaux: applications au microèchangeurs, in: Congrès Français de Thermique, SFT 2005, Reims, 30 May–2 June, 2005.
[24] A.K. Pramanick, P.K. Das, Heuristics as an alternative to variational calculus for the optimization of a class of thermal insulation systems, Int. J. Heat Mass Transfer 48 (2005) 1851–1857.
[25] A. Bejan, M.R. Errera, Convective trees of fluid channels for volumetric cooling, Int. J. Heat Mass Transfer 43 (2000) 3105–3118.
[26] N. Kockmann, T. Kiefer, M. Engler, P. Woias, Channel networks for optimal heat transfer and high throughput mixers, in: ECI International Conference on Heat Transfer and Fluid Flow in Microscale, Castelvecchio Pascoli, Italy, 25–30, September, 2005.
[27] S.W. Kim, S. Lorente, A. Bejan, Vascularized materials: tree-shaped flow architectures matched canopy to canopy, J. Appl. Phys. 100 (2006) 063525.
[28] S. Lorente, A. Bejan, Svelteness freedom to morph, and constructal multiscale flow structures, Int. J. Therm. Sci. 44 (2005) 1123–1130.
[29] C.D. Murray, The physiological principle of minimal work in the vascular system and the cost of blood-volume, Proc. Acad. Natl. Sci. 12 (1926) 207–214.
[30] E.R. Weibel, Symmorphosis: On Form and Function in Shaping Life, Harvard University Press, Harvard, MA, 2000.
[31] J.C. Ordonez, A. Bejan, R.S. Cherry, Designed porous media: optimally nonuniform flow structures connecting one point with more points, Int. J. Therm. Sci. 42 (2003) 857–870.